# Electrochemical Synthesis of 3D Ordered Ferromagnetic Nickel Replicas Using Self-Assembled Colloidal Crystal Templates

Tom S. Eagleton and Peter C. Searson*

*Department of Materials Science and Engineering, Johns Hopkins University, Baltimore, Maryland 21218*

*Received May 24, 2004. Revised Manuscript Received July 30, 2004*

3D ordered nickel replicas of colloidal crystals were fabricated by electrodeposition into colloidal crystal templates. Colloidal crystals were self-assembled in a lateral flow cell that was also used for electrodeposition. We show that 3D replicas with thicknesses up to 100 $\mu$m can be formed over relatively large areas using this approach. We also show that the magnetic properties of the replicas are characteristic of a 3D nanostructured network.

## Introduction

High surface area structures are of interest for a wide range of applications that exploit the high surface-to-volume ratio or the unique properties associated with the small feature sizes in the structure. Disordered or random 3D structures can be formed by aggregation and sintering of particles or by etching one component from a binary alloy system. The fabrication of ordered 3D structures is more challenging but can be achieved by deposition into an ordered colloidal crystal. Ordered 3D replicas have been produced by infiltration of nanometer-sized colloidal particles[1,2] and by electrochemical deposition into colloidal crystal templates.[3−8]

Electrochemical synthesis of 3D ordered structures using a colloidal crystal template is illustrated in Figure 1. In the first step, a crystal is formed on a conducting substrate by self-assembly of particles from suspension. After a suitable plating solution is introduced, the material of interest is electrodeposited into the template. The bottom-up filling of the template results in the formation of a replica of the crystal. Finally, the particles that formed the crystal can be removed by immersion in a suitable solvent or by heating. This technique is more restrictive than infiltration because the crystal template must be assembled on a conducting substrate.

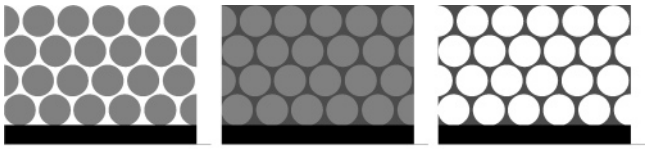


**Figure 1.** Schematic illustration of template-directed synthesis of ordered nanoporous electrodes: (a) self-assembly of ordered crystal from suspension, (b) electrodeposition into crystal template, and (c) removal of template to form an ordered, nanoporous replica.

The self-assembly of three-dimensional crystals can be achieved by sedimentation,[9] flow cell,[10] vertically controlled drying,[11] or templated growth.[12] Conventional sedimentation techniques require a porous substrate and hence are not compatible with subsequent electrodeposition. Controlled drying is also undesirable because the crystals contain macroscopic cracks which result in large volumes of the electrodeposited material in the final structure.

Silica and polymer particles are widely used in the self-assembly of colloidal crystals because they can be easily prepared with narrow size distributions. A disadvantage of silica particles is that assembly can take several months.[5] In contrast, colloidal polystyrene crystals can be produced in a few days.[6,7]

Bartlett et al.[6−8] have used an evaporation technique to form colloidal crystals from polystyrene particles on a conducting substrate and have used electrodeposition to fabricate 3D ordered replicas of several metals, including gold, platinum, palladium, cobalt, and nickel iron alloys. Here, we report on the formation of 3D ordered nickel replicas. Colloidal crystals were formed in a lateral flow cell that was also used for electrodeposition. We show that 3D replicas with thicknesses

* To whom correspondence should be addressed. E-mail: searson@jhu.edu.

(1) Velev, O. D.; Tessier, P. M.; Lenhoff, A. M.; Kaler, E. W. *Nature* **1999**, *401*, 548.
(2) Jiang, P.; Bertone, J. F.; Colvin, V. L. *Science* **2001**, *291*, 453−457.
(3) Braun, P. V.; Wiltzius, P. *Nature* **1999**, *402*, 603.
(4) Jiang, P.; Cizeron, J.; Bertone, J. F.; Colvin, V. L. *J. Am. Chem. Soc.* **1999**, *121*, 7957−7958.
(5) Xu, L.; Zhou, W. L.; Frommen, C.; Baughman, R. H.; Zakhidov, A. A.; Malkinski, L.; Wang, J. Q.; Wiley, J. B. *J. Chem. Soc., Chem. Commun*. **2000**, 997−998.
(6) Bartlett, P. N.; Birkin, P. R.; Ghanem, M. A. *J. Chem. Soc., Chem. Commun*. **2000**, 1671−1672.
(7) Bartlett, P. N.; Baumberg, J. J.; Birkin, P. R.; Ghanem, M. A.; Netti, M. C. *Chem. Mater*. **2002**, *14*, 2199−2208.
(8) Bartlett, P. N.; Ghanem, M. A.; El Hallag, I. S.; De Groot, P.; Zhukov, A. *J. Mater. Chem.* **2003**, *13*, 2596−2602.
(9) Holland, B. T.; Blanford, C. F.; Stein, A. *Science* **1998**, *281*, 538−540.
(10) Park, S. H.; Xia, Y. *Adv. Mater*. **1998**, *10*, 1045.
(11) Jiang, P.; Bertone, J. F.; Hwang, K. S.; Colvin, V. L. *Chem. Mater*. **1999**, *11*, 2132.
(12) van Blaaderen, A.; Ruel, R.; Wiltzius, P. *Nature* **1997**, *385*, 321.

10.1021/cm0491781 CCC: $27.50 
Published on Web 10/16/2004

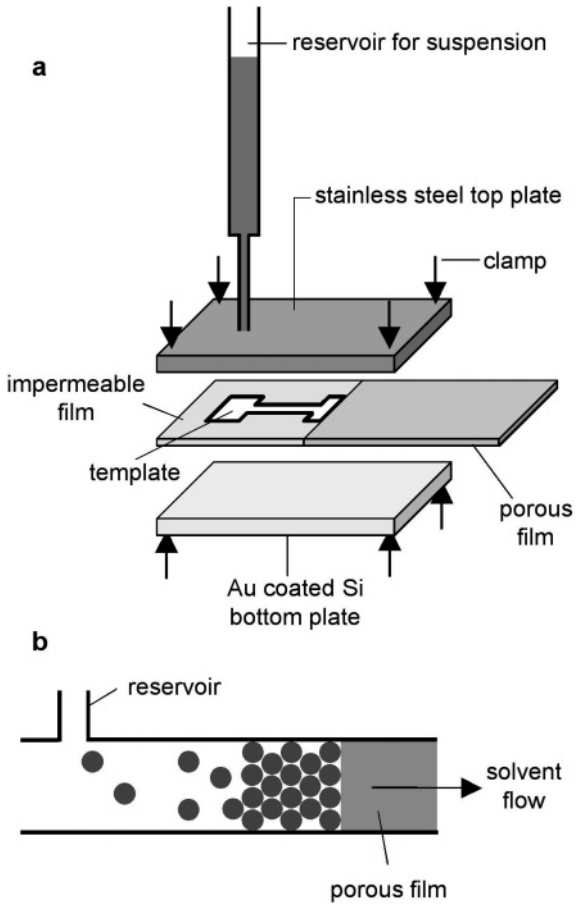


**Figure 2.** (a) Schematic illustration of the cell used for self-assembly and electrodeposition, and (b) cross section of the cell illustrating solvent flow during the self-assembly process.

up to 100 $\mu$m can be formed over relatively large areas using this approach. We also show that the magnetic properties of the replicas are characteristic of a 3D nanostructured network.

## Experimental Methods

Colloidal crystals were assembled using the cell shown in Figure 2. The cell was designed to allow both self-assembly of the crystal and subsequent electrodeposition to be performed sequentially. The cell consisted of a flat substrate and top plate separated by a spacer layer that contained a well for assembly of the crystal. The reservoir for the particle suspension also served as a reservoir for the electrodeposition solution.

The bottom plate of the cell was a Si(100) wafer with a 10 nm Cr adhesion layer and a 100 nm Au layer. The gold layer served as the working electrode during electrodeposition. Prior to each experiment, the stainless steel top plate of the cell was mechanically polished to a mirror finish using SiC paper, ultrasonically cleaned in de-ionized water, and subsequently rinsed in acetone and then isopropanol.

The spacer layer between the top and bottom plates was provided by filter paper (Fisherbrand P8 Grade filter paper, Fisher Scientific). Prior to each experiment, the filter paper was partially immersed in refined paraffin wax (McMaster-Carr) to produce an area impermeable to water. The desired template area was then cut out of the wax-dipped section such that one edge of the template overlapped the remaining permeable region of the filter paper (see Figure 2). The filter paper was selected to have the appropriate pore size to allow flow of the solvent while retaining the particles. The area and shape of the template can be selected according to the required geometry. For experiments reported here, the template area was approximately 0.5 cm$^2$.

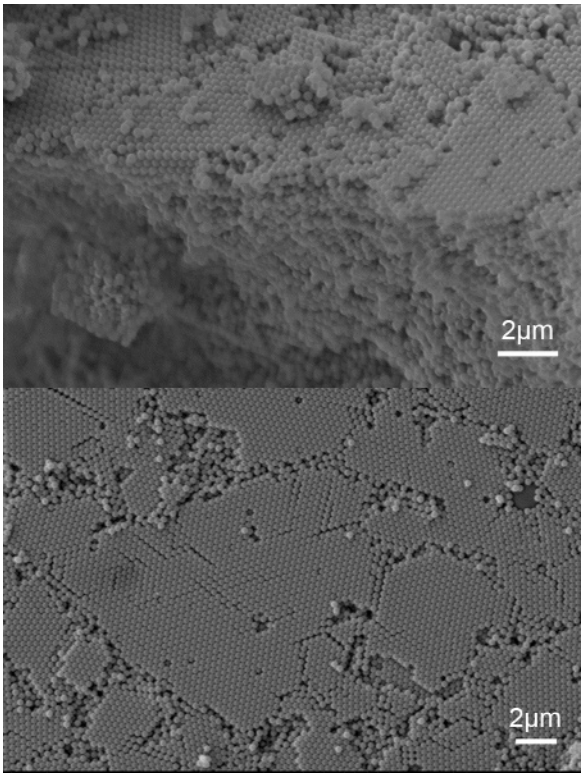


**Figure 3.** SEM images of self-assembled crystal of 500 nm polystyrene particles approximately 10 $\mu$m thick: (a) edge view, and (b) plan view.

During the assembly process, the particles flowed from the reservoir into the template. As the solvent flowed out of the cell through the permeable edge of the filter paper, the particles were concentrated and assembled into an ordered crystal. Colloidal crystals were assembled from polystyrene particles (Polysciences). Three particles sizes were used in the work reported here: 500 nm, 750 nm, and 1 $\mu$m. The average particle sizes, determined from dynamic light scattering measurements (Malvern instruments Zetasizer 3000HSA), were 555 $\pm$ 23, 778 $\pm$ 42, and 1052 $\pm$ 51 nm, respectively. After the suspension was introduced into the reservoir, the cell was placed in a controlled humidity chamber at a relative humidity of 40 $\pm$ 5%. Bulk crystals $\geq$100 $\mu$m thick were typically formed in 5−7 days.

After self-assembly, the remaining suspension was removed and replaced with the electrodeposition solution. Electrodeposition was carried out in a standard three-electrode cell configuration with a platinum wire counter electrode and a 3 M Ag/AgCl electrode reference ($U_{eq}$ = 0.250 V vs SHE) located in the same tube used for the suspension reservoir. Nickel films were deposited from solution containing 1.5 M nickel sulfamate ($Ni(SO_3NH_2)_2$) and 0.5 M boric acid ($H_3BO_3$) adjusted to between pH 3.5 and 4.5. After electrodeposition, the cell was disassembled and the polystyrene particles were removed by immersing the crystal in toluene in an ultrasonic bath.

Scanning electron microscopy (SEM) was carried out using a JEOL 6700FE SEM. Magnetization hysteresis loops were recorded at room temperature using a vibrating sample magnetometer (VSM).

## Results and Discussion

Figure 3 shows scanning electron microscope images of a crystal self-assembled from a suspension of 500 nm polystyrene particles (0.65 wt % solids) in water. The crystal is about 10 $\mu$m thick, corresponding to about 20

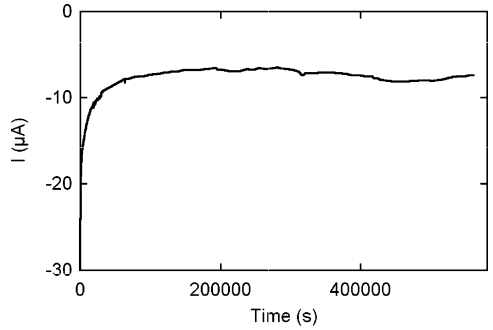


**Figure 4.** Current−time transient for deposition of nickel into a colloidal crystal with 750 nm polystyrene particles. The electrode template area was approximately 0.5 $cm^{-2}$.

particle layers. The plan view image shows good ordering on the top layer of the crystal with domain sizes in the range of 2−10 $\mu$m.

Nickel was electrochemically deposited into the crystals from nickel sulfamate solution at −1.0 V (Ag/AgCl). Figure 4 shows a typical current−time transient for nickel deposition into a crystal with 1 $\mu$m polystyrene particles. The deposition current was typically 10−20 $\mu A\ cm^{-2}$, much smaller than the deposition current for a thin film (typically > 10 $mA\ cm^{-2}$) due to the long diffusion lengths through the crystal. Deposition can take several days, depending on the thickness required. We note that the concentration of nickel ions used for deposition into the crystal templates is higher than that typically used for deposition of thin films.

Figure 5 shows scanning electron microscope images of the top surface of 3D ordered nickel replica formed by deposition into crystals with different particle sizes. The top surface exhibits a negative image of the close-packed surface of the crystal shown in Figure 3. The 3D nickel structures are very robust with no evidence of cracking or deformation during removal of the polystyrene particles. We also note that swelling of the polystyrene particles[13] during immersion in toluene does not cause deformation of the structure.

For an ideal replica, the surface-to-volume ratio $S/V = \pi/2d$, where d is the particle diameter. The specific surface area is then given by $S/Vf\rho$, where $f$ is the volume fraction of solid and $\rho$ is the density. Taking $f = 0.26$ (the atomic packing factor for an fcc or hcp lattice is 0.74) and $\rho = 8.9 \times 10^6\ g\ m^{-3}$ for nickel, the specific surface area ($m^2\ g^{-1}$) for an fcc nickel replica is $6.79 \times 10^{-7}/d$. Thus, for a particle size of 1 $\mu$m, the specific surface area is about 0.7 $m^2\ g^{-1}$. Under ambient conditions, the air-formed oxide on nickel is 1−2 nm thick.[14,15] Thus, although the surface area is relatively high, the oxide only represents about 1% of the volume of the solid phase.

Figure 6 shows a cross section of an electrodeposited nickel replica fabricated from a colloidal crystal with 750 nm polystyrene particles. The nickel structure is about 130 particles or 100 $\mu$m thick. The film thickness is in good agreement with the thickness obtained from the deposition charge, assuming a volume fraction of 0.26 and a deposition efficiency of 1.0. The structure is well ordered from the substrate to the free surface with preferred (111) texture. Similar results were reported by Bartlett et al.[7] for polystyrene crystals self-assembled by evaporation.

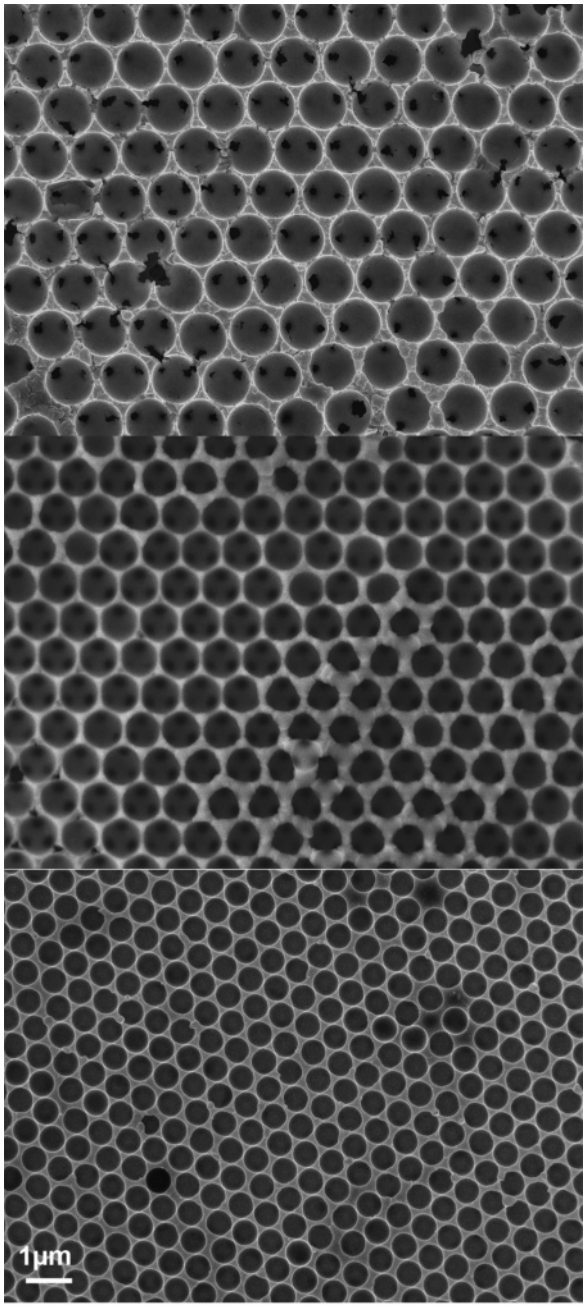


**Figure 5.** Plan view scanning electron microscope images of 3D ordered nickel structures deposited into templates assembled from (a) 1 $\mu$m, (b) 750 nm, and (c) 500 nm polystyrene particles. The polystyrene particles have been removed by ultrasonic immersion in toluene. The crystals were approximately 10 $\mu$m thick.

The backscattered electron image of the interface region shows good adhesion between the gold substrate and the deposited nickel. There is no evidence of residual polystyrene, illustrating that the porous network percolates throughout the crystal allowing complete removal of the polystyrene particles, even over relatively long distances.

From the plan view images shown in Figure 5, it is apparent that the topmost plane of cells in the replica

(13) Habicht, J.; Schmidt, M.; Ruhe, J.; Johannsmann, D. *Langmuir* **1999**, *15*, 2460−2465.
(14) Sato, N.; Kudo, K. *Electrochim. Acta* **1974**, *19*, 461−470.
(15) Scherer, J.; Ocko, B. M.; Magnussen, O. M. *Electrochim. Acta* **2003**, *48*, 1169−1191.

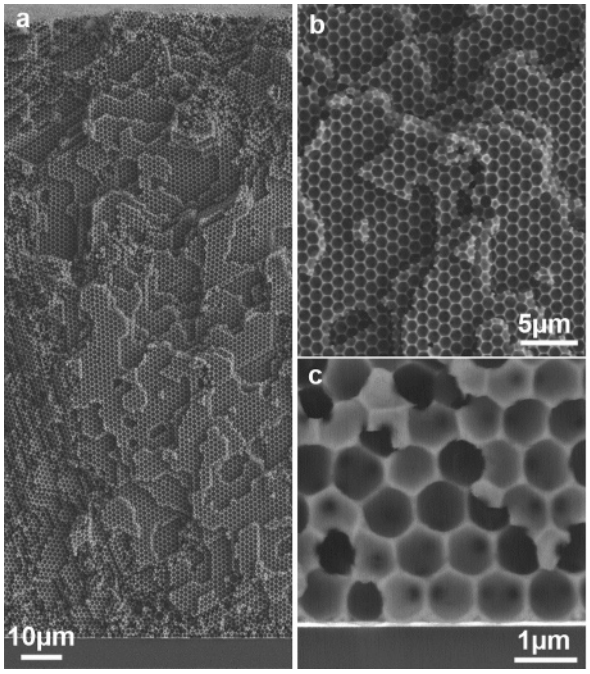


**Figure 6.** Cross-section SEM images of 3D ordered nickel replica: (a) full cross section, (b) enlargement of region in the middle of the film, and (c) enlargement of region near substrate. The colloidal crystal template was assembled from 750 nm polystyrene particles.

exhibits a close-packed structure. Each cavity formed by the polystyrene particles has three dark spots corresponding to the contact points with the three particles in the layer below. The symmetry shows that the particles are located in three-fold hollow sites in the crystal. In some images, it was possible to identify the position of three sequential close-packed layers with respect to each other. As shown in Figure 7a, in most cases, the ordering corresponds to the ABCABC stacking associated with an fcc crystal. In some instances, ABAB stacking characteristic of hcp crystals was also observed, as shown in Figure 7b. Theoretical calculations[16] have shown that the fcc structure is the lowest energy state, although there is a relatively small energy difference between the fcc and hcp structures.

The surface of the colloidal crystals is usually the (111) surface, as expected from self-assembly under near-equilibrium conditions. Occasionally, other orientations are also seen. Figure 8 shows a (100) domain on the surface of a nickel replica.

Figure 9b shows an FFT of a high magnification scanning electron microscope image (12 × 8 $\mu$m) of a nickel replica formed by deposition into a template with 1 $\mu$m diameter polystyrene particles (Figure 9a). Because this image is of a single domain of close-packed cells, the image is characterized by a spot pattern with three-fold symmetry. The FFT of the low magnification image (60 × 40 $\mu$m) shown in Figure 9d shows a ring pattern due to the multiple domains in the image (Figure 9c). Figure 9e shows intensity versus $q$ plots obtained from the FFTs. The curves for both high and low magnification images show peaks up to the tenth nearest neighbor. From the peak spacing, we obtain a near neighbor spacing of 1075 nm, very close to the

(16) Woodcock, L. V. *Nature* **1997**, *385*, 141−143.

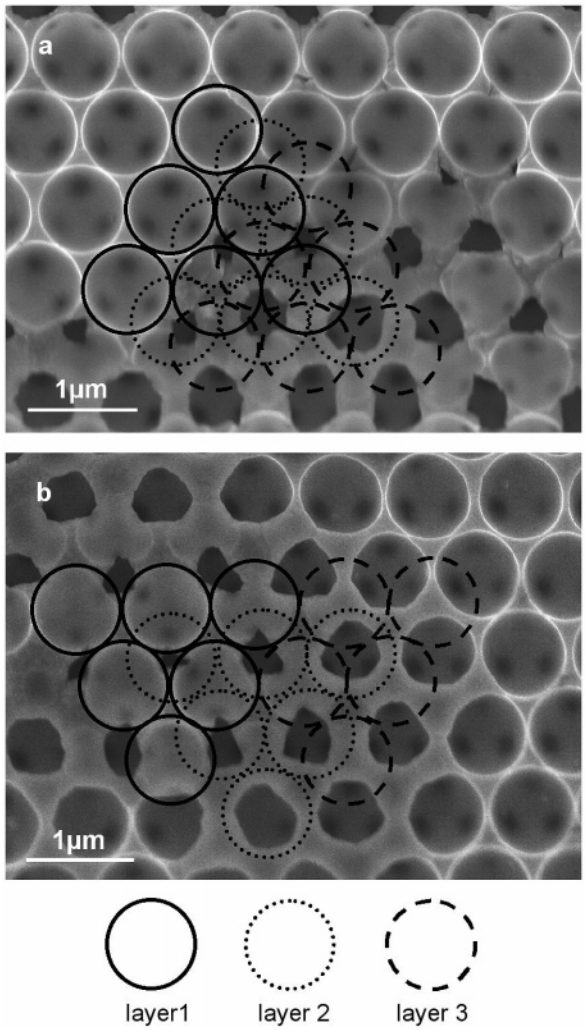


**Figure 7.** Plan view SEM images of the surface of 3D ordered nickel replicas fabricated by deposition into a template assembled from 750 nm diameter polystyrene particles: (a) fcc structure, and (b) hcp structure. The surface exhibits a (111) orientation, and cells in planes parallel to the surface are indicated by circles.

particle size obtained from dynamic light scattering (1052 ± 51 nm) and from SEM images of crystal templates (1055 ± 21 nm).

The distribution of particle sizes leads to a distribution of cell sizes in the nickel replica, and hence the introduction of a variety of defects. Figure 10 shows plan view SEM images of nickel replicas, illustrating a vacancy completely filled with nickel and an interstitial in the surface. Figure 10 also shows a large cell formed by a large polystyrene particle in the original crystal template.

The structure of the 3D replicas gives rise to some unusual properties in comparison to bulk materials. Figure 11 shows $M-H$ loops for a 3D ordered nickel replica and an electrodeposited nickel film. With the applied magnetic field in the film plane, the nickel film exhibits a relatively square loop with a high remanence ($M_r/M_s = 0.67$) characteristic of the magnetic easy axis. With the magnetic field perpendicular to the film plane, the loop is sheared which is characteristic of the magnetic hard axis. Because nickel exhibits a small magnetocrystalline anisotropy, the magnetic response is expected to be dominated by the shape anisotropy.

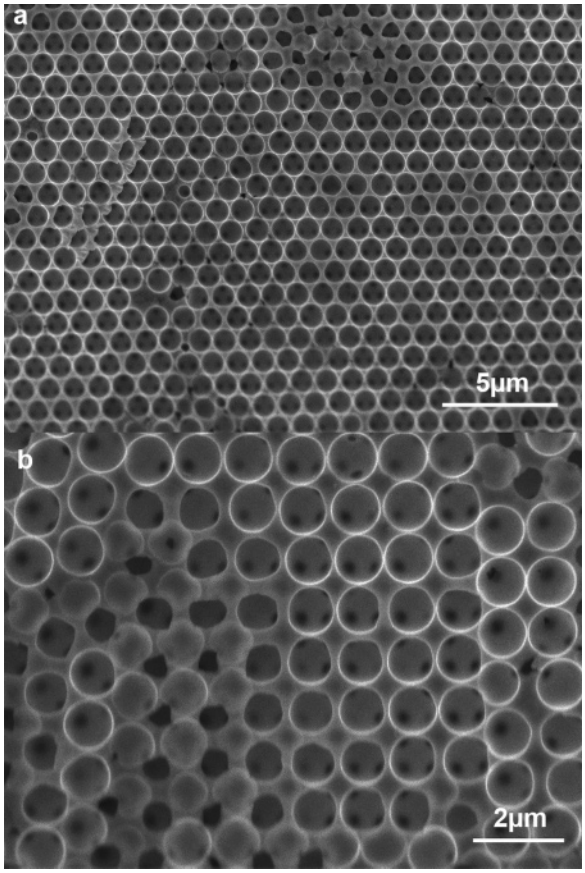


**Figure 8.** Plan view SEM images of the surface of 3D ordered nickel replicas: (a) large (111) domain (>25 × 20 $\mu$m), and (b) a (100) domain.

The saturation field for the nickel film along the hard axis is close to the value of $4\pi M_s = 6095$ Oe expected from the demagnetization factor for a thin film,[17] illustrating that magnetocrystalline anisotropy is negligible.

The $M-H$ loop for the nickel replica with the magnetic field parallel to the film plane is more sheared with a much lower remanence ($M_r/M_s = 0.35$) than for the electrodeposited thin film. Furthermore, with the magnetic field perpendicular to the film plane, the $M-H$ loop is noticeably less sheared than for the electrodeposited thin film and has a remanence $M_r/M_s = 0.10$. These features illustrate that the 3D replica is much more isotropic than the electrodeposited film.

The coercivity of the nickel replica is 109 Oe with the applied field parallel to the film plane and 164 Oe with the applied field perpendicular to the film plane. The coercivity of the replica is considerably larger than that for the nickel film (90 ± 1 Oe with the applied field parallel or perpendicular to the film plane) and is related to the 3D structure. Bartlett et al.[8] have also reported an enhancement in coercivity for 3D nickel and cobalt replicas. Switching in small single domain magnetic nanostructures, such as nanowire arrays,[18,19] is often characterized by a large size-dependent increase in the coercivity. A similar increase in coercivity has been reported for 2D ferromagnetic network structures[20−23] due to domain wall pinning caused by the nonuniform structure.

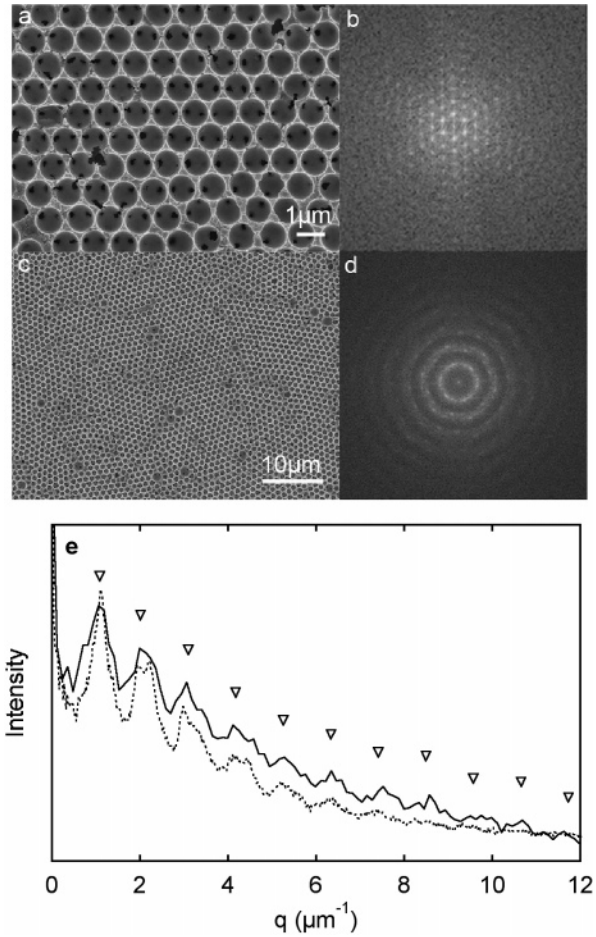


**Figure 9.** (a) High magnification plan view SEM image of nickel replica fabricated by deposition into a template assembled from 1 $\mu$m diameter polystyrene particles and (b) FFT of image. (c) Low magnification SEM image of the same nickel replica and (d) corresponding FFT of image. (e) Intensity versus $q$ plot of FFTs obtained at high magnification (solid line) and low magnification (dotted line). The lattice spacing obtained from the peaks is 1.075 $\mu$m.

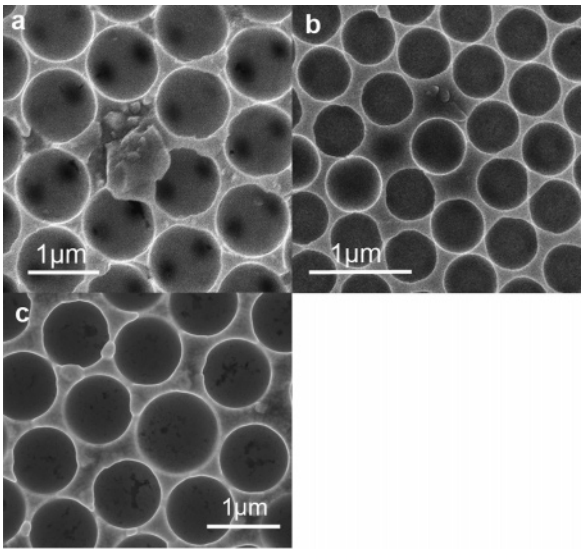


**Figure 10.** Plan view SEM images of defects in the nickel replicas: (a) vacancy, (b) interstitial, and (c) locally distorted lattice due to large particle.

(17) Cullity, R. D. *Introduction to Magnetic Materials*; Addison-Wesley: Reading, MA, 1972.
(18) Sun, L.; Searson, P. C.; Chien, C. L. *Appl. Phys. Lett.* **1999**, *74*, 2803.
(19) Sun, L.; Searson, P. C.; Chien, C. L. *Appl. Phys. Lett.* **2001**, *79*, 4429.

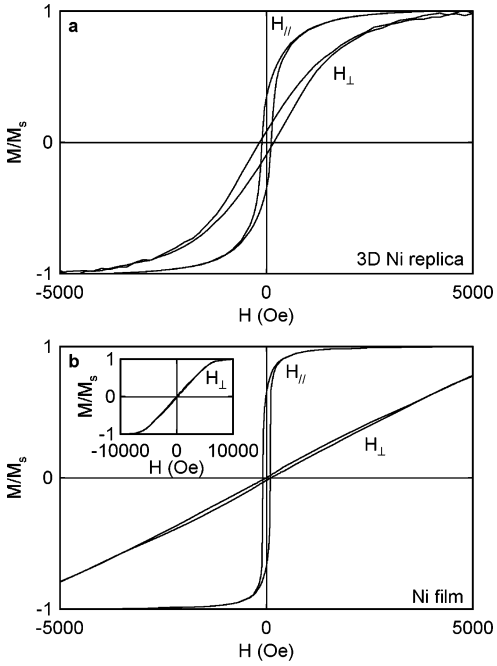


**Figure 11.** *M*−*H* curves for (a) 3D ordered nickel replica with the applied field parallel and perpendicular to the film plane, and (b) for an electrodeposited nickel film with the applied field parallel and perpendicular to the film plane. The inset shows the complete hysteresis loop with the applied field perpendicular to the film plane. The 3D ordered nickel replica was fabricated by deposition into a template with 1-$\mu$m diameter polystyrene particles. Measurements were obtained at room temperature.

In bulk ferromagnetic materials, the energy of the system can be minimized by forming multiple magnetic domains in which the atomic magnetic moments are aligned. However, in nanostructured magnetic materials, there is a critical size below which a particle remains in a single domain state during switching. A rod-shaped nickel particle with an aspect ratio of 10 would be expected to be single domain for diameters less than about 600 nm, whereas cobalt and iron particles with the same aspect ratio would be expected to be single domain for diameters less than about 140 nm.[24] From Figures 5 and 6, it is clear that the triangular regions between three cells in the replicas are on the order of 200 nm, suggesting that the 3D nickel replica can be considered as a network of small, single domain nanometer scale ligaments.

The switching mode in a nanostructure is determined by the competition between the exchange energy and the demagnetization energy. For intermediate particle sizes, typically 10−20 nm[25] up to the single domain limit, magnetization reversal can be approximated by the curling model, where the coercivity is dependent on both particle size and aspect ratio. The increase in coercivity reported for the Ni replica is expected to be related to curling in a network of single domain ligaments. In this regime, the coercivity and switching fields are strongly dependent on particle size; for a rod-shaped particle and in the absence of other effects, the coercivity can increase with the inverse square of the particle radius.[24] We note that when the particle dimensions decrease below 5−20 nm, the coercivity decreases with decreasing particle size as the superparamagnetic limit is approached. This effect has been observed in 2D networks.[23] These results suggest that the magnetic properties of 3D replicas can be tuned over a wide range by changing the particle size in the crystal template or by changing the spacing between particles.

## Summary

We have demonstrated that 3D replicas with thicknesses up to 100 $\mu$m can be formed over relatively large areas. Colloidal crystals were formed by self-assembly of polystyrene particles in a lateral flow cell that was also used for electrodeposition. From the replicas, we determine that the colloidal crystals were predominantly fcc with a preferred (111) texture. The magnetic properties of the 3D replica are more isotropic than for a nickel film and exhibit enhanced coercivity that is attributed to domain wall pinning in the nickel network.

**Acknowledgment.** This work was supported by the ARL PEER program.

CM0491781

(20) Barnard, J. A.; Fujiwara, H.; Inturi, V. R.; Jarratt, J. D.; Scharf, T. W.; Weston, J. L. *Appl. Phys. Lett.* **1996**, *69*, 2758.
(21) Liu, K.; Chien, C. L. *IEEE Trans. Magn*. **1998**, *34*, 1021.
(22) Liu, K.; Baker, S. M.; Tuominen, M.; Russell, T. P.; Schuller, I. K. *Phys. Rev. B* **2001**, *63*, 060403.
(23) Sun, L.; Ding, Y.; Chien, C. L.; Searson, P. C. *Phys. Rev. B* **2001**, *64*, 184430.
(24) Frei, E. H.; Shtrikman, S.; Treves, D. *Phys. Rev*. **1957**, *106*, 446.
(25) Aharoni, A. *Introduction to the Theory of Ferromagnetism*; Oxford University Press: New York, 1996.